Journal of Nuclear Materials 415 (2011) S104–S107

Contents lists available at ScienceDirect

Journal of Nuclear Materials

journal homepage: www.elsevier.com/locate/jnucmat

Nanostructure formation on tungsten exposed to low-pressure rf helium plasmas: A study of ion energy threshold and early stage growth

M.J. Baldwin *,[1], T.C. Lynch, R.P. Doerner, J.H. Yu

University of California at San Diego, CA 92093-0417, USA

ARTICLE INFO

Article history:
Available online 2 November 2010

ABSTRACT

Nanostructure formation on W targets is explored as a function of He^+ impact energy, ε_i, in the range $20 \leqslant \varepsilon_i \leqslant 57$ eV. Six targets are exposed at 1120 K for 6 h to pure He plasmas, generated by a low-pressure rf Helicon source. One target is additionally exposed to Ar plasma pre-treatment. It is found that He ions of impact energy 32–37 eV are necessary for nanostructure formation to be observed in this type of plasma, as determined by SEM. At 57 eV a nanostructured surface forms readily (similar to that observed by Baldwin and Doerner, Nuclear Fusion 48 (2008) 035001 in the PISCES–B device), but growth is retarded in the Ar pre-treatment case. Thermal desorption shows that nanostructuring is accompanied by increased trapping of He in degenerate vacancies and clusters, but is reduced by a factor of 8 as a result of Ar pre-treatment.

1. Introduction

High temperature (>900 K) exposure of W to energetic He produces a surface layer of disordered nanoscopic 'rod-like' features, roughly 10–50 nm thick and up to a micron in length [1,2]. The nanoscopically structured layer is not limited to the near surface, but grows in thickness as long as the W remains in contact with the source of ionized He [2]. The action of He accumulated in W vacancies and defects, leading to bubbles, combined with high temperature W mobility [3] is gaining acceptance as the interplay of mechanisms that lead to this effect, but as yet an understanding of nanostructure growth is far from complete. W nanostructure formation presents issues very relevant to W divertor operation in JET, ITER and next generation reactors. The potential for surface exfoliation/dust production leading to core contamination, modified erosion/material loss properties and reduced thermal performance are just a few open issues that could lead to adverse performance of a fusion device. As such, the He–W interaction at high temperature has increasingly become the subject of ITER divertor research and development activity. In this article we focus on the development of He induced nanostructure morphology at its early stages, and its dependence on ion-impact energy, in order to better understand the mechanisms that control its formation.

2. Experimental

W targets used in this experiment were disks, 25 mm in diameter and 1.5 mm thick, cut from a rolled W plate (W–99.97 wt.%) supplied by Plansee USA. In order to investigate surface features on the nanometer scale, each target was ground and polished with a final lap using 1 μm diamond suspension. The resulting average surface roughness, R_a, was typically better than 10 nm as measured using a Dektak IIA stylus profilometer. Polished W targets were then exposed to 1 kW plasmas through He in an inductively-coupled plasma reactor utilizing a version of the Trikon M0Ri™ Helicon source driven at 13.56 MHz. An analysis of the plasma properties achievable in this device is given in Taylor et al. [4].

Six targets were individually exposed to He plasma at a temperature of 1120 K for 6 h. One target was exposed also to an in situ Ar plasma pre-treatment at 600 K for 2 h prior to He plasma exposure. Targets were electrically biased from floating potential V_f to −33 V to study the effect of ion bombardment at various energies. In these plasmas the Debye length, λ_D is 7.7×10^{-5} m and the ion–neutral collision free path is of the order of 0.1 m, which allows the target–plasma sheath potential to be equated with the impact-energy of impinging ions. The sheath potential was inferred from the analysis of data from a single rf-compensated probe designed to suppress the rf drive frequency and its first harmonic [4], and the ion energy distribution was additionally examined using a Hiden Analytical EQP energy analyzer [5].

Subsequent to plasma exposure, targets were examined for surface-nanostructure growth with a JEOL–JSM 6360 scanning-electron microscope (SEM), and then further analyzed using the

* Corresponding author. Address: UCSD Center for Energy Research, 9500 Gilman Drive, La Jolla, CA 92093-0417, USA.
E-mail address: mbaldwin@ferp.ucsd.edu (M.J. Baldwin).
[1] Presenting author.

0022-3115/$ - see front matter © 2010 Elsevier B.V. All rights reserved.
doi:10.1016/j.jnucmat.2010.10.050

technique of thermal desorption mass spectrometry (TDS). During TDS, targets are outgassed by heating at a linear rate of 0.6 K s^{-1} up to 1900 K inside a Veeco-Applied High-Temperature-Effusion Cell. The $m/e = 4$ (He) partial pressure–time profile, as measured by SRS RGA-100 residual gas analyzer, is concurrently recorded.

3. Results

To explore the nanostructure formation dependence on He^+ ion energy, exposure plasmas were measured with an electrical probe and an ion-energy spectrometer. Fig. 1a shows a single probe IV characteristic taken in close proximity to the target, but outside of the target–plasma sheath. The inset shows determination [6] of the plasma ion density n_{He+} as 6.3×10^{16} m^{-3}. Fig. 1b shows the electron current collected by the probe (ion saturation subtracted) and yields values of the electron temperature T_e, density n_e, and plasma potential V_p, to be 6.5 eV, 6.0×10^{16} m^{-3} and 24.2 V respectively [7]. The linearity of Fig. 1b reveals that the exposure plasma chosen exhibits little to no hot electron population, and this is further evidenced in the electron energy distribution function (EEDF) of Fig. 1c deduced from the data of Fig. 1b using the Druyvestein method [6], further fit with a single Maxwellian distribution. Fig. 1d shows the distribution of ion energies in the He plasma adjusted in the plot (centered at V_p) to reflect the ion energy spectrum from the target perspective. As is common in rf plasmas, the distribution is bimodal due to parasitic capacitive coupling [8]. A grounded target would thus experience He^+ impact events of energy ε_{i0}, ~24 eV with spread at half maximum of 6.5 eV, and a target biased to V_b that of $\varepsilon_i = \varepsilon_{i0} + qV_b/e$ where $q/e = 1$.

Fig. 2 shows normal incidence SEM images of the targets exposed in this study. The images of Fig. 2a and b, where ε_i was 20 eV (V_b = floating) and 27 eV (V_b = –3 V) respectively, show little convincing evidence that the W surfaces developed a morphological change after 6 h of He plasma exposure. However, for ε_i = 32 eV (V_b = –8 V), Fig. 2c, evidence of sub-micron scale 'grooves' are observed that appear to have directional properties over areas consistent with the average grain size. As ε_i is further increased the size-scale of surface features is reduced. Fig. 2d, where ε_i = 37 eV (V_b = –13 V), displays surface features reduced in size and with additional evidence of pinholes. Pinholes occur at the center of surface features and also within grooves, thereby acting to 'breakup' or reduce the size-scale of larger features. In a separate study using a transmission electron microscope TEM [9] the grooves are suggested to be due to the action of clustering/percolating nanobubbles, a phenomena also observed for He ion bombardment of other metals [10,11], but too small to observe with the SEM used

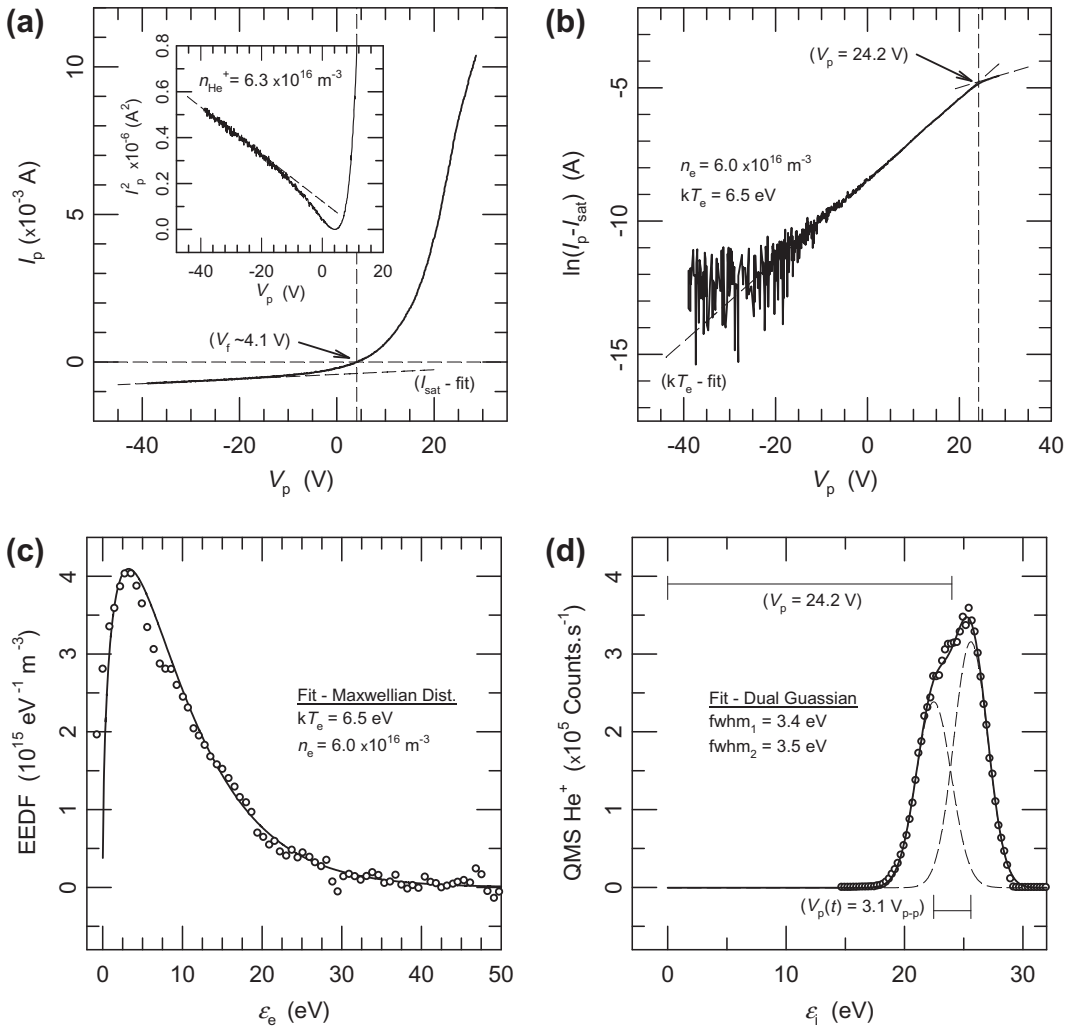

Fig. 1. (a) Single probe IV characteristic showing fitted ion saturation current. Inset shows determination [5] of plasma ion density $n_{He}^{+} = 6.3 \times 10^{16}$ m^{-3}, (b) probe electron current (ion saturation subtracted). T_e, n_e and V_p are to be 6.5 eV, 6.0×10^{16} m^{-3} and 24.2 V, respectively, (c) EEDF deduced from (b) using the Druyvestein method, further fit with a single Maxwellian distribution [6] and (d) the distribution of ion energies measured with a Hiden EQP ion-energy spectrometer and adjusted to reflect the ion spectrum from the target perspective.

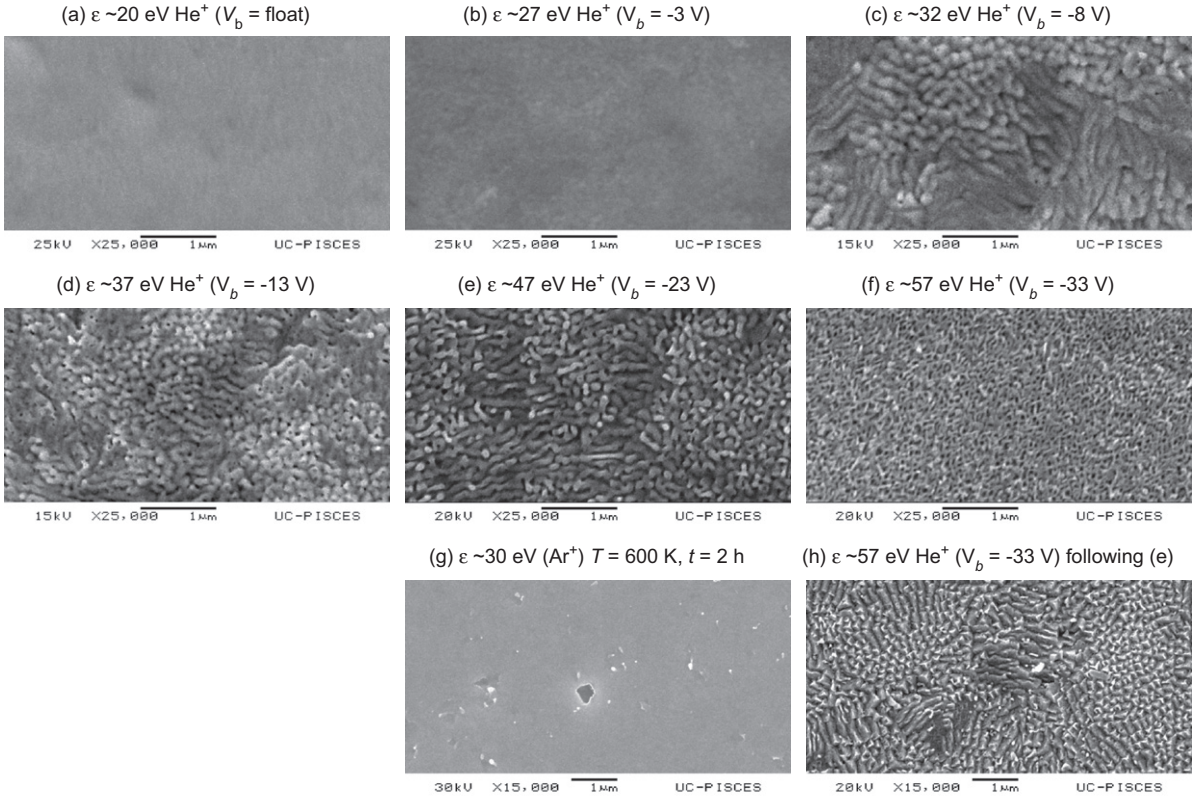

Fig. 2. SEM images of plasma exposed W targets taken at normal incidence. The target–plasma exposure conditions are $T_e = 6.5$ eV, $n_{He}^{+} = 6.3 \times 10^{16}$ m^{-3}, $\Gamma_{He^+} = 4.0 \times 10^{20}$ m^{-2} s^{-1}, $T = 1120$ K and $t = 6$ h, respectively. Ion-impact energy regimes were (a) $\varepsilon_i = 20$ eV (no change), (b) $\varepsilon_i = 27$ eV (no change), (c) $\varepsilon_i = 32$ eV (grooving), (d) $\varepsilon_i = 37$ eV (grooving and pinholes), (e) $\varepsilon = 47$ eV (towards nanostructure), (f) $\varepsilon_i = 57$ eV (nanostructure), (g) Ar plasma pre-treatment at 600 K for 2 h and (h) $\varepsilon_i = 57$ eV (retarded structuring) following (g).

in these experiments. In Fig. 2e, where $\varepsilon_i = 47$ eV ($V_b = -23$ V), the grooved and broken up features are beginning to grow away from the W surface and in Fig. 2f, $\varepsilon_i = 57$ eV ($V_b = -33$ V), surface features are fully reminiscent of the W nanostructuring that is found with elevated temperature exposure of W to He plasma in high flux linear-plasma devices [1,2]. Lastly we reveal an interesting observation; the exposed W surface of Fig. 2h, $\varepsilon_i = 57$ eV ($V_b = -33$ V). This target was exposed to similar He plasma conditions as the other targets and ought to show a nanostructured surface morphology, as in Fig. 2f. Its morphology, however, is more like that of Fig. 2c implying at least retarded nanostructure growth. The difference is due to a pre-treatment in Ar plasma at 600 K for 2 h, Fig. 2g, that was carried out to study any possible effect due to Ar bombardment, since Ar may be used as an extrinsic radiator in the ITER divertor.

Fig. 3 shows He TDS profiles for a selection of targets imaged in Fig. 2. He release from W has long been studied [12] and it is known that thermal release with temperature is characterized by first order depopulation of trap sites, such as vacancies and clusters, filled with a multiplicity of He. Vacancy binding $He_{n'}$–V gives rise to release peaks indicated H, G, F, E, in Fig. 3, and for increasing multiplicity (but $n' < \sim 10$), the desorption peak temperature falls as the vacancy fills. However, at about $n' \sim 10$ the filled vacancy displaces neighboring W atoms leading to He filled clusters with higher binding energy than the original vacancy complex. At this point, desorption is characterized by trap release that shifts to higher temperature ($\sim$1800 K) as the cluster continues to fill. A highly degenerate He filled cluster is the immediate precursor to the formation of a He bubble. The desorption profiles of Fig. 3 depict a superposition of both vacancy and cluster bound He release. The profiles, which are progressively offset and arranged in order of increasing ion energy show a general trend. The reduction in scale size of surface features from sub-micron towards nanostructure, as depicted in Fig. 2, corresponds in the TDS profiles of Fig. 3, to increased levels of desorption from $He_{n'=2-10}$–V complexes and increasingly degenerate He filled clusters. In the first instance, this is apparent from the increasing trend in peak heights associated with $He_{n'=2-10}$–V release, and in the second, the general shifting of cluster peaks from $\sim$1600 K to $\sim$1800 K. Accordingly, the total release of He from the target also increases, from 2.2×10^{21} He m^{-2} for $\varepsilon = 20$ eV, to 6.7×10^{21} He m^{-2} at $\varepsilon_i = 57$ eV. In the Ar pre-treatment case, the observation of retarded morphology growth, Fig. 2h, is reflected also in the TDS release profile as there is no convincing release from $He_{n'=2-10}$–V peaks, and reduced release and temperature shift in cluster associated peaks. Further, the total release was only 8.8×10^{20} He m^{-2}, a factor of 8 or so less than the companion $\varepsilon_i = 57$ eV target that did not undergo pre-treatment and exhibited a nanostructured surface.

4. Discussion and conclusion

Nanostructure is known to grow efficiently on W above 900 K [13] in plasma devices with a high flux of energetic He species [1,2,13]. However, it is unclear the precise energy that incident species require to initiate growth and difficult to investigate in high power plasma devices like [2] where the target temperature is coupled to the plasma generation. A low-pressure rf plasma allows independent control over incident-ion energy and target tem-

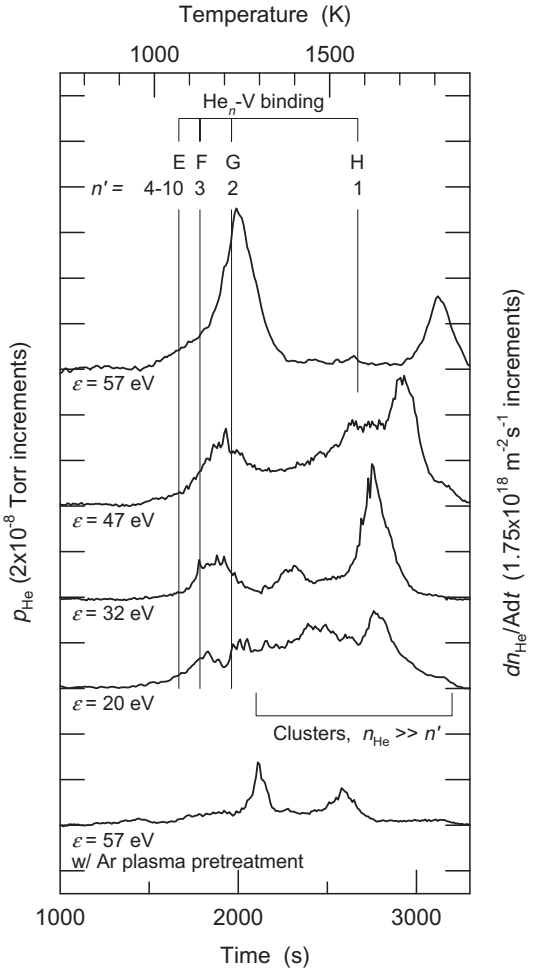

Fig. 3. Plot of TDS profiles for He plasma exposed W targets. Profiles are shown for W targets exposed to ion impact energies of $\varepsilon_i = 20$ eV (no change), $\varepsilon_i = 32$ eV (grooving), $\varepsilon_i = 47$ eV (towards nanostructure) $\varepsilon_i = 57$ eV (nanostructure) and $\varepsilon_i = 57$ eV but with prior Ar plasma pre-treatment at 600 K for 2 h.

perature and, as shown in Fig. 1a–d, offers quiescent plasma conditions defined by a single Maxwellian electron temperature with a well defined plasma–target sheath.

At face value, W targets exposed to this type of plasma do infact give the impression of an energy threshold for the formation of surface nanostructure, as shown in Fig. 2a–f. Comparison of Fig. 2b and c suggest that incident He ions must have sufficient energy of 32–37 eV (adjusted for ~5 eV spread, Fig. 1d) in order for nanostructure to grow. This agrees well with recent observations made by Kajita et al. [14] on W exposed >1000 K to He plasma in NAGDIS–II. Nanostructure was found to form efficiently for ions of ~50 eV, but at 15 eV only pinholes were noted. Since this threshold energy range is well below that necessary for He to produce damage induced traps in the W [15], it is intriguing exactly what role ion energy plays. In the range 20–50 eV [16] the stopping range for He in W increases from ~10 to 20 Å while the He reflection coefficient decreases from 0.75 to 0.68 (the incident ion flux is essentially constant) so it can only be speculated that increased ion energy leads to deeper implantation and that nanostructure growth proceeds by self-driven mechanisms related to surface saturation with He.

The TDS data of Fig. 3 further corroborate this view. Increased He-ion energy is shown to lead to increased levels of release from filled $He_{n'=2-10}$–V complexes and clusters, but it is interesting to note that even the $\varepsilon_i = 20$ eV case showed He accumulation in the target despite the absence of surface featuring or nanostructure. Thus, in view of all the data, it would seem that energetic ions, above the threshold energy of 32–37 eV, are important for nanostructure formation at low He ion fluxes (E.g., $\Gamma_{He^+} = 4.0 \times 10^{20}$ m^{-2} s^{-1} here), but it cannot be ruled out that nanostructure formation may proceed below this threshold at higher incident-ion fluxes since the necessary accumulation of He also occurs below our measured threshold.

On a final note, there is the observation of retarded nanostructuring, and reduced He inventory in the Ar plasma pre-treated target. In studies by Kornelsen and Gorkum [12], He is less strongly bound to vacancies implanted by noble gas species compared to He–V, and the desorption from $He_{n'=2-10}$–(Ne, Ar, Kr, Xe)V traps proceeds at considerably lower temperatures as the mass of the noble gas atom increases. In the case of Ar, $He_{n'=2-10}$–ArV traps desorb below ~850 K, significantly below the formation temperature of nanostructure >900 K [13]. On the other hand, He filled vacancies do not depopulate until above ~1000 K, so it is speculated that Ar plasma pre-treatment, in occupying some fraction of near surface (<5 Å) vacancies, may act to reduce the efficiency of He uptake by continual thermal release during the He plasma exposure. Or alternatively, an additional hypothesis might be that Ar pre-treatment sputter cleans the surface of impurities, thereby reducing impurity nucleation sites for He accumulation. Either way, further work is necessary to determine the role of Ar in retarding fuzz growth.

Acknowledgements

The authors wish to acknowledge PISCES–B beryllium enclosure personnel. This work is supported by a USDoE Grant Award: #DE-FG02-07ER54912.

References

[1] S. Takamura, N. Ohno, D. Nishijima, S. Kajita, Plasma Fusion Res. 51 (2006) 1.
[2] M.J. Baldwin, R.P. Doerner, Nucl. Fusion 48 (2008) 035001.
[3] E. Lassner, W. Schubert, Tungsten – Properties, Chemistry, Technology of the Element, Alloys and Chemical Compounds, Springer-Verlag, 1999.
[4] K.J. Taylor, S. Yun, G.R. Tynan, J. Vac. Sci. Technol. A 22 (5) (2004) 2131.
[5] E. Oyarzabal, J.H. Yu, R.P. Doerner, G.R. Tynan, K. Schmid, J. Appl. Phys. 100 (2006) 063301.
[6] I. Langmuir, H.M. Mott-Smith, Gen. Electr. Rev. 27 (1924) 449.
[7] V.A. Godyak, R.B. Piejak, B.M. Alexandrovich, Plasma Sources Sci. Technol. 1 (1992) 36.
[8] D. Barton, D.J. Heason, R.D. Short, J.W. Bradley, Meas. Sci. Technol. 11 (2000) 1726.
[9] M. Miyamoto, D. Nishijima, M.J. Baldwin, R.P. Doerner, Y. Ueda, Y. Yasunaga, N. Yoshida, K. Ohno, P3-95, these proceedings.
[10] P.B. Johnson, D.J. Mazey, J. Nucl. Mater. 93–94 (2) (1980) 721.
[11] H. Scher, R. Zallen, J. Chem. Phys. 53 (1970) 3759.
[12] E.V. Kornelsen, A.A. Van Gorkum, J. Nucl. Mater. 92 (1980) 79.
[13] M.J. Baldwin, R.P. Doerner, D. Nishijima, K. Tokunaga, Y. Ueda, J. Nucl. Mater. 390–391 (2009) 886.
[14] S. Kajita, W. Sakaguchi, N. Ohno, Plasma Dev. Oper. 17 (2) (2009) 165.
[15] H.H. Neely, D.W. Keefer, A. Sosin, Phys. Stat. Solidi. 28 (1968) 675.
[16] W. Eckstein, Calculated sputtering, Reflection and Range Values, Max–Planck Institut für Plasmaphysik Report 9/17, 1998.